Reconstruction of current profile parameters and plasma shapes in tokamaks

1985 Nucl. Fusion 25 1611

(http://iopscience.iop.org/0029-5515/25/11/007)

RECONSTRUCTION OF CURRENT PROFILE PARAMETERS AND PLASMA SHAPES IN TOKAMAKS

L.L. LAO, H. St. JOHN, R.D. STAMBAUGH,
A.G. KELLMAN, W. PFEIFFER
GA Technologies, Inc.,
San Diego, California,
United States of America

ABSTRACT. An efficient method is given to reconstruct the current profile parameters, the plasma shape, and a current profile consistent with the magnetohydrodynamic equilibrium constraint from external magnetic measurements, based on a Picard iteration approach which approximately conserves the measurements. Computational efforts are reduced by parametrizing the current profile linearly in terms of a number of physical parameters. Results of detailed comparative calculations and a sensitivity study are described. Illustrative calculations to reconstruct the current profiles and plasma shapes in ohmically and auxiliarily heated Doublet III plasmas are given which show many interesting features of the current profiles.

1. INTRODUCTION

External magnetic measurements in tokamaks have provided important information on plasma shapes, global current profile parameters, such as the sum of the average poloidal beta $\bar{\beta}_p$ and half the plasma internal inductance ℓ_i, and for sufficiently elongated plasmas $\bar{\beta}_p$ and ℓ_i separately [1–3].

When the available information is limited to external magnetic measurements alone, only global parameters of the current profile can be determined. An efficient method to reconstruct the plasma shapes and the line integrals of the boundary poloidal magnetic field from external magnetic measurements was presented by Swain and Neilson [4]. In this approach, the plasma current distribution is approximated by using a few filament currents. It has been shown that the method can accurately determine most of the limited and diverted plasma shapes produced in Doublet III [3]. For plasmas which are large enough to simultaneously touch the top, the inner limiter and the outer limiter, and whose current distributions are broad, the method becomes inaccurate.

A more complete and accurate approach was described by Luxon and Brown [5]. In their approach, the plasma currents are modelled using distributed sources. In addition to the plasma shapes, the sum of $\bar{\beta}_p$ and $\ell_i/2$, and for sufficiently elongated plasmas $\bar{\beta}_p$ and ℓ_i separately, this method also yields a current profile consistent with the magnetohydrodynamic (MHD) equilibrium constraint. However, the computational effort involved is extensive and requires repeatedly solving the non-linear Grad-Shafranov equation to search for the best-fit current density profile. Since large amounts of experimental data must be routinely processed, it is highly desirable to have an alternative, fast, yet sufficiently accurate, method to determine the plasma shapes and the global current profile parameters. For Doublet III, it is further required that the method be capable of handling both limited and diverted plasmas.

This paper presents a method which can be used to efficiently reconstruct the current profile parameters, the plasma shapes, and a current density profile satisfying the MHD equilibrium constraint, based on a Picard iteration approach which approximately conserves the external magnetic measurements. Computational efforts are reduced by parametrizing the current profiles linearly in terms of a number of parameters describing $\bar{\beta}_p$, ℓ_i, the total plasma current I_0, and the axial safety factor q_0, and by interleaving the fitting and the equilibrium iterations. The original non-linear optimization problem is transformed into a sequence of linearized minimizations interleaved with the equilibrium iterations, which is easily solved using the singular value decomposition method. This method of solving linear least-square minimization problems is less sensitive to truncation errors and uncertainty in measurement data and, therefore, is particularly suited to handle ill-conditioned problems such as this one. The reconstruction equally treats the measured poloidal fluxes and all other signals using their appropriate

measurement errors and does not require any knowledge of the poloidal flux ψ along the boundary of the computational domain. Both diverted and limited plasmas can be well handled. The method is particularly useful for tokamaks with an air core such as Doublet III. An efficient method, based on a different finite-element algorithm and specifically useful for tokamaks with an iron core such as the Joint European Torus (JET), is given in Ref.[6]. This method requires a knowledge of ψ along the boundary of the computational domain which is obtained by interpolating the measured poloidal flux values. The measured fluxes are treated as absolutely correct, even though in reality there are always measurement errors associated with them. This method also reduces the computational effort by interleaving the fitting and the equilibrium iterations.

To demonstrate the capability of our method to accurately reconstruct the plasma shapes and global current profile parameters, detailed comparative calculations and sensitivity studies are performed using simulated as well as measured Doublet III magnetic signals. It is shown statistically that, if the current profile parametrization is physically reasonable, the reconstructed current profile closely describes the gross features of the actual distribution, although not its fine structure. Secondly, the reconstructed global current profile parameters, such as $\bar{\beta}_p$ and ℓ_i, depend only very weakly on the form of the current parametrization used and the value of the axial safety factor q_0 imposed, as expected theoretically. Illustrative calculations to reconstruct the plasma shapes and current profiles in ohmically and auxiliarily heated Doublet III plasmas are also given, showing many interesting features of the current profiles.

In Section 2, the Picard iteration method is described. Results of comparative calculations, a sensitivity study and some applications of the method are given in Section. 3. Conclusions are summarized in Section 4.

2. PICARD ITERATIONS

It is known that from external magnetic measurements alone, only global parameters of the current profile, such as the total plasma current I_0, the sum of $\bar{\beta}_p$ and $\ell_i/2$, and for sufficiently elongated plasmas $\bar{\beta}_p$ and ℓ_i separately, can be determined [1–3]. This section describes a method based on the Picard iteration approach to efficiently determine these parameters from external magnetic measurements making use of the MHD equilibrium constraint.

A particular method to compute MHD equilibria is the Green's function approach. The equilibrium Grad-Shafranov equation $\Delta^*\psi = -8\pi^2 R J_t/c$ is first recast into the integral form, making use of the toroidal Green's function $G(\bar{r},\bar{r}')$, and the solution is then obtained by Picard iterations [7–9]:

$$\psi^{(m+1)}(\bar{r}) = \sum_{n=1}^{n_e} G(\bar{r},\bar{r}_{en}) I_{en} + \int_{\Omega^{(m)}} dR'dZ'\, G(\bar{r},\bar{r}') J_t(R',\psi^{(m)}) \qquad (1)$$

where ψ is the poloidal flux, m denotes the iteration cycle, n_e is the number of external shaping coils, I_{en} is the current strength of the n-th external coil located at $\bar{r}_{en}$, Ω is the plasma volume, and J_t is the toroidal current density,

$$J_t = 2\pi c R\left[P'(\psi) + \frac{F^{2\prime}(\psi)}{2\pi c^2 R^2}\right] \qquad (2)$$

Here, P is the plasma pressure, F is the poloidal current, and cgs Gaussian units are used.

For a rectangular computational domain, ψ at the interior points may alternatively be obtained by inverting the Δ^* operator using the fast Buneman's method and the Picard iteration scheme [7–10]:

$$\Delta^*\psi^{(m+1)} = -\frac{8\pi^2 R}{c} J_t(R,\psi^{(m)}) \qquad (3)$$

To obtain physically desired equilibria, during the course of the iterations the current density profile is continuously adjusted in order to conserve global plasma parameters such as the total plasma current I_0 and the axial safety factor q_0.

In an experimental situation, J_t is not known, but rather it is parametrized in terms of a number of parameters which are to be determined from the measured external magnetic signals. The fact that there is no unique way to represent J_t reflects that only global parameters of the current density profile can be determined in this case, although, once the current model has been chosen, the parameters can generally be uniquely determined. Here, to reduce the computational effort, a simple model for J_t is chosen. The two free functions $P'(\psi)$ and $F^{2\prime}(\psi)$ are modelled as polynomials in ψ, with linear coefficients α_n and β_n, to be determined from the measured signals and the imposed constraints

$$P'(\psi) = \sum_{n=0}^{n_P} \alpha_n x^n - x^{n_P+1} \sum_{n=0}^{n_P} \alpha_n \tag{4}$$

$$F^{2\prime}(\psi) = \sum_{n=0}^{n_F} \beta_n x^n - x^{n_F+1} \sum_{n=0}^{n_F} \beta_n \tag{5}$$

where $x = (\psi - \psi_M)/(\psi_B - \psi_M)$ varies between 0 and 1, ψ_M is the poloidal flux at the magnetic axis, ψ_B is the boundary poloidal flux, and P' and $F^{2'}$ are taken to be zero at the boundary. The total number of coefficients $n_P + n_F + 2$ are chosen according to the number of global current parameters that can be determined from the available measurements and the number of constraints imposed.

For example, in Doublet III the available measurements are the poloidal fluxes near the shaping coils, the poloidal magnetic fields at fixed locations surrounding the plasma, the total plasma current, and the diamagnetic flux. It is known from external magnetic field measurements that for elongated plasmas $\bar{\beta}_p$ and ℓ_i can be separately determined and for nearly circular plasmas only the sum $\bar{\beta}_p + \ell_i/2$ can be determined [1–3]. Thus, if the axial safety factor q_0 is additionally constrained to have a given value, for elongated plasmas the current density profile may be parametrized in terms of four parameters, describing I_0, $\bar{\beta}_p$, ℓ_i and q_0, which are to be determined from the external poloidal flux, field and total current measurements. For nearly circular plasmas, the diamagnetic flux measurement must be used additionally in order to obtain $\bar{\beta}_p$ and ℓ_i separately. Empirically, it has been found that the current density profile in Doublet III can be well modelled by

$$P'(\psi) = \alpha_0 + \alpha_1 x + \alpha_2 x^2 - (\alpha_0 + \alpha_1 + \alpha_2) x^3 \tag{6}$$

$$F^{2\prime}(\psi) = \beta_0 (1 - x) \tag{7}$$

During the iteration cycles, the parameters α_n, β_n and I_{en} are readjusted continuously, according to the available signals and the imposed constraints, by finding the solution to a linearized minimization problem which minimizes

$$\chi^2 = \sum_{i=1}^{n_M} \left(\frac{M_i - C_i}{\sigma_i} \right)^2 + \sum_{i=1}^{n_C} \left(\frac{H_i - D_i}{\zeta_i} \right)^2 \tag{8}$$

where M_i, C_i and σ_i denote the measured value, the computed value and the error associated with the i measurement, and H_i, D_i and ζ_i denote the given value, the computed value and the uncertainty associated with the i constraint. The poloidal fluxes, the poloidal magnetic fields and the total current corresponding to the measurements are computed according to the Picard iteration scheme:

$$C_i^{(m+1)}(\bar{r}_i) = \sum_{n=1}^{n_e} G_{C_i}(\bar{r}_i, \bar{r}_{en}) I_{en}^{(m+1)} + \int_{\Omega^{(m)}} dR' dZ' G_{C_i}(\bar{r}_i, \bar{r}') J_t(R', \psi^{(m)}; \alpha_n^{(m+1)}, \beta_n^{(m+1)}) \tag{9}$$

where G_{C_i} is the appropriate Green's function corresponding to the i measurement. Similarly, the diamagnetic flux $\Delta\phi$ corresponding to the measurement is computed according to the linearized scheme

$$\Delta\phi^{(m+1)} = \frac{1}{cF_0} \int_{\Omega^{(m)}} dR dZ \frac{[F_0^2 - F^2(\psi^{(m)}; \beta_n^{(m+1)})]}{R} \tag{10}$$

where $F_0 = cB_{t0}R_0/2$ and B_{t0} is the vacuum toroidal magnetic field at R_0. The constraints imposed are linearized in a similar fashion. For example, the axial safety factor q_0 is approximated as

$$\frac{1}{q_0^{(m+1)}} = \frac{2\pi E_M^{(m)} (R_M^{(m)})^2}{F(0)^{(m)}[(E_M^{(m)})^2 + 1]} \times \left(2\pi c R_M^{(m)} \alpha_0^{(m+1)} + \frac{\beta_0^{(m+1)}}{c R_M^{(m)}} \right) \tag{11}$$

where E_M and R_M are the elongation at the magnetic axis and the major radius of the magnetic axis.

The merit figure describing the reconstruction, χ^2, can then be rewritten as

$$\chi^2 = \| \vec{\vec{L}} \vec{y} - \vec{b} \| \tag{12}$$

where $\| \cdots \|$ denotes the norm of a vector, the unknown vector $\vec{y}$ consists of the external currents I_{en} and the parameters α_n and β_n, and the vector $\vec{b}$ consists of the external measurements and the constraint values which are normalized by their corresponding uncertainty. The response matrix $\vec{\vec{L}}$, linearly relating the unknowns

to the normalized measurements and constraints, is an appropriate rearrangement of the Green's functions and their integrations over the plasma volume (Appendix).

The linearized minimization problem is then easily solved using the singular value decomposition method by orthogonally factoring the response matrix $\vec{\vec{L}}$ into a diagonal matrix $\vec{\vec{Q}}$[11]. The method is less sensitive to truncation errors and uncertainty in measurement data and, therefore, is particularly suited to handle ill-conditioned problems such as this one. Providing the diagonal elements of $\vec{\vec{Q}}$ are not zero, the solution to the linearized minimization problem is unique. Thus, by transforming the original non-linear optimization problem into a sequence of linearized minimizations interleaved with the equilibrium iterations, the computational effort is substantially reduced. In contrast to the standard approach, where typically a number of equilibrium calculations are performed to find the best-fit current profile, the number of iterations involved now is of the order of that required to find a single equilibrium.

The external coil currents I_{en} may be treated as given, making use of their measured values. However, since in reality there are always errors associated with the measurements, it is better to treat the I_{en} as unknowns determined by matching to the measured currents as well as using all other available data. In Doublet III, only the measured poloidal magnetic fluxes at the external shaping coils are used for two reasons. First, the fluxes can be measured more accurately than the currents. Secondly, the eddy currents flowing in the vacuum chamber can be somewhat accounted for by requiring the fluxes at the shaping coils rather than the currents to be matched in the reconstruction.

3. COMPARATIVE CALCULATIONS AND SENSITIVITY STUDY

3.1. Comparative calculations

To demonstrate the capability of this method to accurately reconstruct the plasma shapes and the current density profile parameters for tokamaks, detailed comparative calculations using the Doublet III configuration are given in this section.

The magnetic diagnostics of Doublet III used in the calculations are shown in Fig.1. They consist of 24 flux loops, 12 partial Rogowski coils, 11 magnetic probes, and 1 full Rogowski coil. There are 24 external poloidal shaping coils. Two kinds of comparisons are

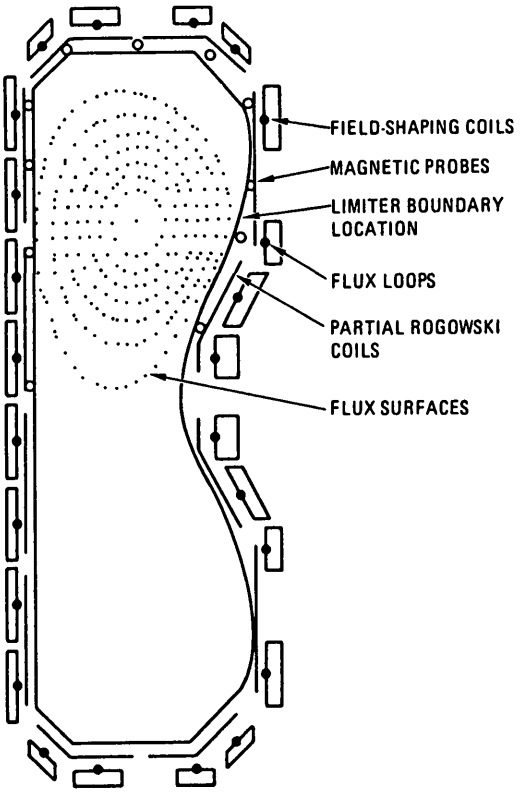

FIG.1. Magnetic diagnostics of Doublet III.

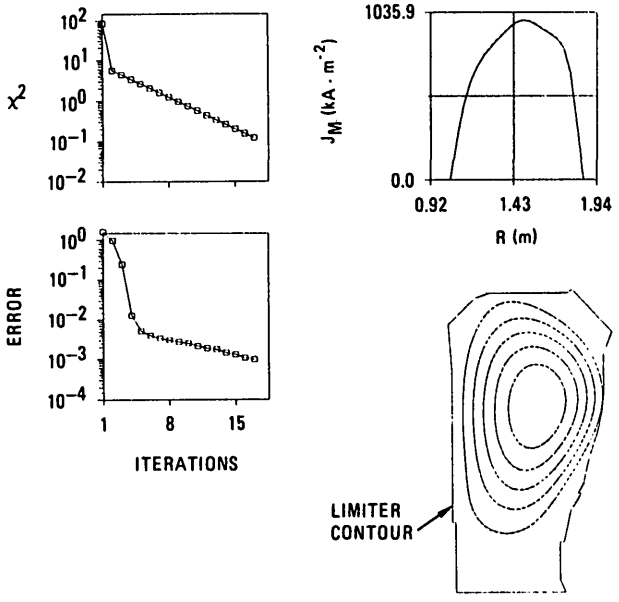

FIG.2. Comparison of the reconstructed calculations with the exact results for a limited Doublet III plasma. The dashed lines are the exact results.

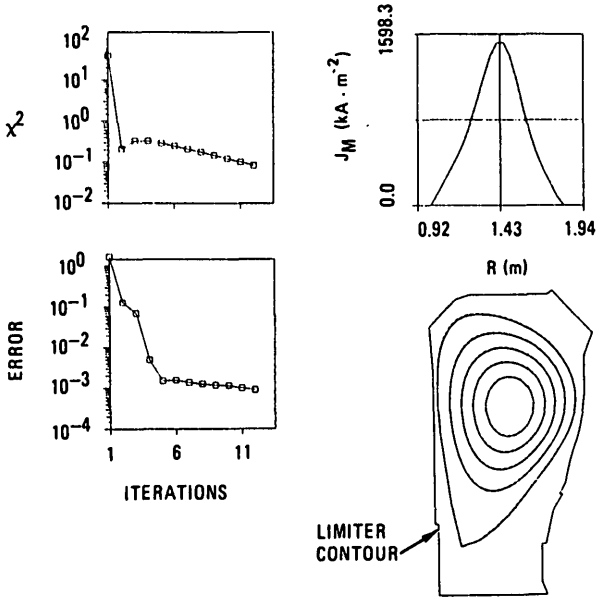

FIG.3. Comparison of the reconstructed calculations with the exact results for a diverted Doublet III plasma. The dashed lines are the exact results.

given. In the first type, magnetic signals at the probes are simulated using a standard equilibrium code. In the second type, actual measured Doublet III magnetic data are used.

In Figs 2 and 3, the results of two reconstructed calculations are compared with the exact results from the equilibrium calculations. In Fig.2, the reconstructed magnetic surfaces and the toroidal current density at the horizontal plane passing through the magnetic axis, J_M, are compared with the exact equilibrium results for a high toroidal beta limited dee-shaped plasma. The dashed lines represent the exact equilibrium calculations using a standard equilibrium code. The current profile is taken to be polynomials of ψ as given in Eqs (6) and (7) and is adjusted during the equilibrium calculation to give fixed values of the total plasma current I_0 and the axial safety factor q_0. The parameters are summarized in Table I. The solid lines in Figs 2 and 3 represent the results of the reconstructed calculation. The magnetic signals at the measuring probes are simulated from the results of the equilibrium calculation. Additionally, q_0 is constrained to have the given value of 0.95. The current profile is parametrized linearly in terms of four parameters as given in Eqs (6) and (7). The reconstructed global plasma parameters, such as $\bar{\beta}_p$, ℓ_i, the average toroidal beta $\bar{\beta}_t$, I_0, the boundary safety factor q_ℓ, the plasma volume Ω, the average major radius $R_g = (R_{max}+R_{min})/2$, the average vertical position $Z_g = (Z_{max}+Z_{min})/2$, the minor radius $a = (R_{max}-R_{min})/2$, and the average elongation $E = (Z_{max}-Z_{min})/2a$, are compared with the exact values in Table I. The agreement between the reconstructed and the exact results is excellent. In this case, the plasma current model well describes the actual current distribution. Thus, the reconstructed current profile and the internal magnetic surfaces are in excellent agreement with the exact results. Also shown in Fig.2 are the evolution of χ^2 and the maximum relative error of ψ during the iterations. Both χ^2 and the relative ψ error decrease rapidly as the iterations proceed. Similarly, the reconstructed results for a diverted Doublet III plasma are compared with the exact equilibrium results in Fig.3 and in Table I. Again, the agreement is excellent. In this case, the equivalent safety factor q^* [12], instead of q_ℓ, is given in Table I.

The reconstructed plasma shapes and global current profile parameters depend very weakly on the current profile model chosen and the value of q_0 imposed. These are illustrated in Tables II and III and in Figs 4 and 5. The cases where the modelled plasma current profile does not completely describe the actual current distribution are considered in Figs 4 and 5 and in Table II. Again, the dashed lines represent the exact results from the equilibrium calculation; in this case, they are generated using the toroidal current density profile of the form

$$J_t = J_0 \left[\beta_{c0}\frac{R}{R_c} + (1-\beta_{c0})\frac{R_c}{R}\right](1-x^n)^m \qquad (13)$$

where $P'(\psi)$ and $F^{2'}(\psi)$ are taken to be proportional and to have similar profiles, $\beta_{c0} = 0.89$, $m = 0.63$, $R_c = 1.43$ m, and J_0 and n are adjusted during the equilibrium iterations to give $I_0 = 472$ kA and $q_0 = 0.95$. In all cases, the solid lines represent the reconstructed calculations. Again, the magnetic signals to the measuring probes are simulated from the results of the equilibrium calculation. In Fig.4(a), the plasma current profile is modelled in the shape of polynomials of ψ as given in Eqs (4) and (5) with $n_P = 3$ and $n_F = 1$. In all cases, q_0 is constrained to be 0.95. Similarly, in Figs 4 (b) and 4 (c), the plasma current profiles are modelled with $n_P = n_F = 2$ and $n_P = 1$ and $n_F = 3$, respectively. In Fig.5(a), the plasma current is modelled by constraining $P'(\psi)$ and $F^{2'}(\psi)$ to be proportional to each other,

TABLE I. COMPARISON OF RECONSTRUCTED AND EXACT RESULTS USING IDENTICAL CURRENT PROFILE PARAMETRIZATIONS

		$\bar{\beta}_p$	ℓ_i	$\bar{\beta}_t$ (%)	q_ℓ/q^*	Ω (m^3)	R_g (cm)	Z_g (cm)	a (cm)	E	I_0 (kA)	q_0	α_0	α_1	α_2	β_0
Limited	Exact	0.81	0.78	3.60	2.51	6.93	144.8	74.1	40.5	1.59	466.8	0.95	1.00	−0.71	2.16	1.04
Dee-shaped	Reconstructed	0.81	0.77	3.59	2.51	6.93	144.8	74.4	40.5	1.59	465.8	0.95	1.00	−0.77	2.31	1.03
Diverted	Exact	0.50	1.29	0.34	6.65	6.24	140.6	68.4	40.0	1.61	293.5	0.95	1.00	−3.10	3.83	1.14
	Reconstructed	0.49	1.30	0.34	6.63	6.23	140.7	68.2	40.0	1.61	294.1	0.95	1.00	−3.05	3.73	1.15

TABLE II. COMPARISON OF RECONSTRUCTED AND EXACT RESULTS USING DIFFERENT CURRENT PROFILE PARAMETRIZATIONS

	$\bar{\beta}_p$	ℓ_i	$\bar{\beta}_t$ (%)	q_ℓ	Ω (m^3)	R_g (cm)	Z_g (cm)	a (cm)	E	I_0 (kA)	q_0
Exact	0.91	0.77	4.22	2.46	6.85	145.1	74.0	40.2	1.59	472.3	0.95
$n_P = 3$ $n_F = 1$	0.91	0.76	4.21	2.47	6.87	145.1	74.2	40.2	1.60	471.8	0.95
$n_P = 2$ $n_F = 2$	0.89	0.74	4.17	2.39	6.77	145.2	74.3	40.1	1.58	472.3	0.95
$n_P = 1$ $n_F = 3$	0.90	0.75	4.20	2.43	6.82	145.2	74.1	40.2	1.59	472.2	0.95
Proportional $n_P = 3$	0.91	0.76	4.20	2.46	6.86	145.1	74.2	40.2	1.59	471.9	0.95
Proportional $n_P = 2$	0.91	0.76	4.20	2.47	6.88	145.1	74.1	40.3	1.59	472.3	1.18

TABLE III. COMPARISON OF RECONSTRUCTED AND EXACT RESULTS USING DIFFERENT CURRENT PROFILE PARAMETRIZATIONS AND DIFFERENT q_0

	$\bar{\beta}_p$	ℓ_i	$\bar{\beta}_t$ (%)	q_ℓ	Ω (m^3)	R_g (cm)	Z_g (cm)	a (cm)	E	I_0 (kA)
Exact $q_0 = 0.95$	0.91	0.77	4.22	2.46	6.85	145.1	74.0	40.2	1.59	472.3
$q_0 = 0.5$	0.90	0.78	4.18	2.43	6.80	145.2	74.2	40.1	1.59	471.4
$q_0 = 2.0$	0.92	0.75	4.20	2.51	6.94	145.0	74.0	40.3	1.60	473.0

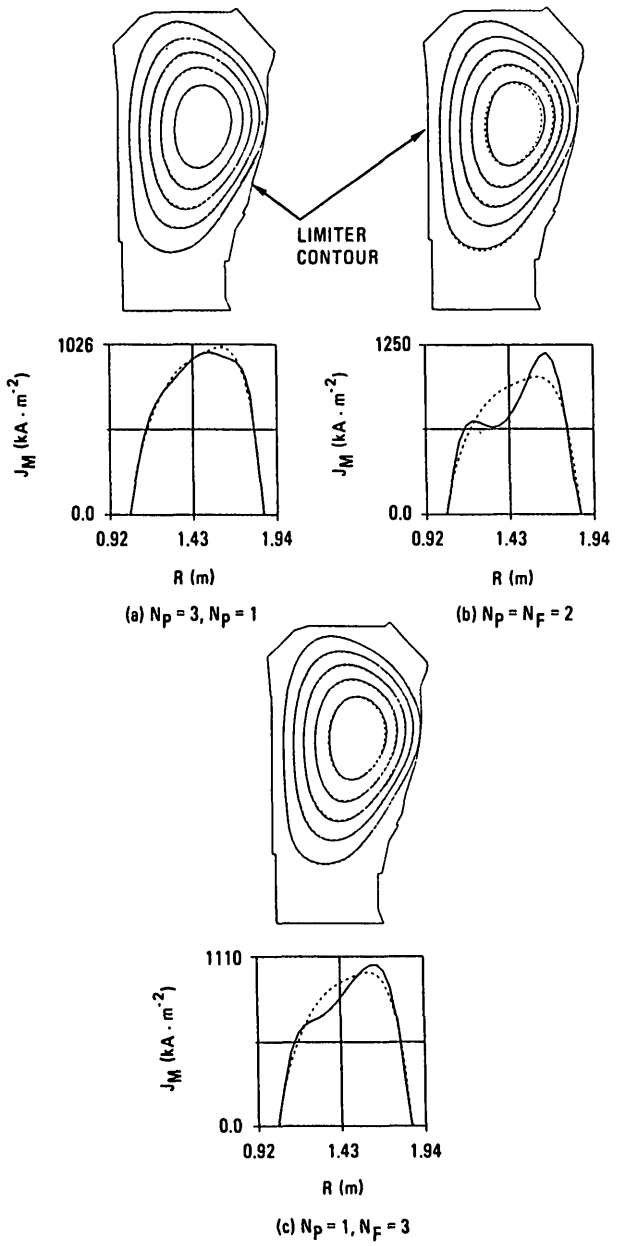

FIG.4. Comparison of the reconstructed calculations with the exact results for a limited Doublet III plasma using different current profile models. The dashed lines are the exact results.

$$J_t = 2\pi c \left[\beta_{c0}\frac{R}{R_c} + (1-\beta_{c0})\frac{R_c}{R}\right] \times \left(\sum_{n=0}^{n_P} \alpha_n x^n - x^{n_P+1}\sum_{n=0}^{n_P}\alpha_n\right) \qquad (14)$$

where $n_P = 3$. Again, q_0 is constrained to be 0.95. In Fig.5(b), the plasma current is again modelled using Eq.(14), except that q_0 is not constrained to have any given value and $n_P = 2$. In this case, q_0 has a fitted value of 1.18, whereas the exact value is 0.95. Of all the current profile parametrizations, the choices given in Eqs (6) and (7) and in Eq.(14) provide the best description of the original current profile. All models yield values of $\bar{\beta}_p$ and ℓ_i within 4% of each other. The cases where the constrained value of q_0 differs from the actual one are examined in Table III. The reconstructed global plasma parameters agree closely with the exact values.

It was mentioned earlier that the fast filament plasma current method developed by Swain and Neilson [4] can accurately reproduce many of the limited and diverted plasma shapes produced in Doublet III [3], but when the plasma is large and simultaneously touches the top, the inner limiter and the outer limiter, and when the current distribution is broad, the method becomes inaccurate. This is illustrated in Fig.6, where the reconstructed plasma boundary surfaces from the MFIT code, which is based on the filament current model [3], and the EFIT code, which is based on the Picard iteration method described above and which uses the distributed current model as given in Eqs (6) and (7), are compared with the exact results from the equilibrium calculation. Again, the

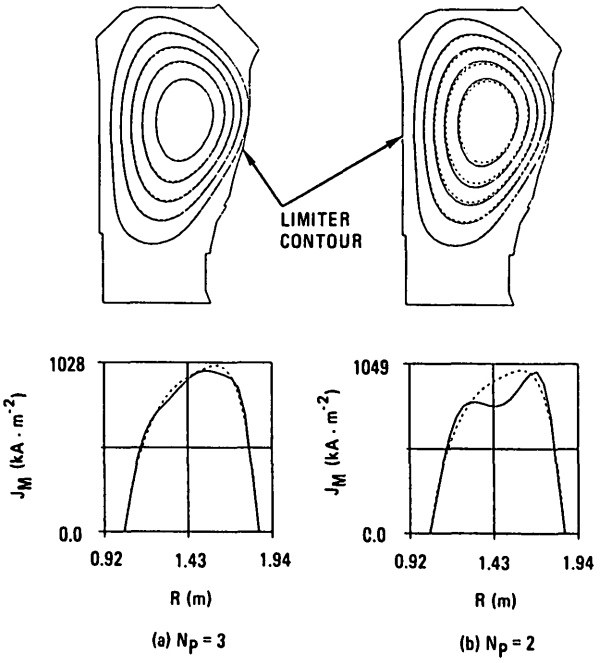

FIG.5. Comparison of the reconstructed calculations with the exact results for a limited Doublet III plasma. The dashed lines are the exact results. $P'(\psi)$ and $F^{2'}(\psi)$ are constrained to be proportional to each other.

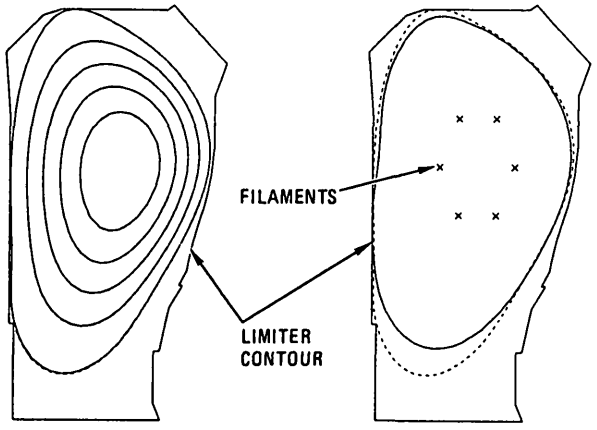

FIG.6. Comparison of the reconstructed plasma shapes (using the filament plasma current model and the distributed current model) with the exact results. The dashed lines are the exact results.

solid lines represent the reconstructed results and the dashed lines represent the exact equilibrium results. The global plasma parameters are compared in Table IV. Of particular concern are the elongation E, the plasma volume Ω, and the safety factor at the boundary q_ℓ, which have the exact values of 1.73, 8.01 m^3, and 3.93, respectively. The filament method yields $E = 1.58$ and $\Omega = 7.38$ m^3, whereas the distributed current method yields $E = 1.73$ and $\Omega = 7.98$ m^3. However, because of the strong dependence of q_ℓ on E, the filament method yields $q_\ell = 3.01$, whereas the distributed current method yields $q_\ell = 3.89$.

In the remainder of this section, a second type of comparison, using the actual measured Doublet III magnetic data, is considered. In Table V, the global plasma parameters for a number of high $\bar{\beta}_t$ limited

TABLE IV. COMPARISON OF RECONSTRUCTED RESULTS USING FILAMENT AND DISTRIBUTED CURRENT MODELS WITH THE EXACT RESULTS

	Ω (m^3)	R_g (cm)	Z_g (cm)	a (cm)	E	q_ℓ	I_0	$\bar{\beta}_p$	ℓ_i	$\bar{\beta}_t$ (%)
Exact	8.01	141.2	69.5	42.7	1.73	3.93	728.9	1.12	0.88	3.87
MFIT Filament model	7.38	140.5	73.6	42.4	1.58	3.01	730.6	1.01	0.86	4.01
EFIT Distributed model	7.98	141.2	69.7	42.7	1.73	3.89	728.4	1.12	0.88	3.89

TABLE V. COMPARISON OF HIGH-BETA RESULTS

Shot	Time (ms)	$\bar{\beta}_p$		$\bar{\beta}_t$		Elongation		Volume (m^3)		q_ℓ	
		EFIT	GAQ	EFIT	GAQ	EFIT	GAQ	EFIT	GAQ	EFIT	GAQ
37946	830	0.95	0.89	4.29	4.10	1.62	1.56	6.92	6.76	2.54	2.38
39330	818	0.99	0.98	4.06	4.01	1.48	1.46	6.40	6.34	2.44	2.41
39400	800	1.02	1.03	4.20	4.18	1.44	1.44	6.21	6.20	2.35	2.34
41989	910	1.00	1.02	4.02	4.15	1.42	1.41	6.66	6.58	2.46	2.38
43481	875	1.03	1.06	4.33	4.35	1.48	1.49	6.00	6.02	2.22	2.46
49490	900	0.97	0.95	4.11	4.11	1.47	1.43	6.03	5.80	2.16	2.05
43492	875	0.79	0.76	4.00	4.10	1.55	1.48	6.50	6.10	2.13	1.91
43493	875	0.84	0.76	4.29	4.18	1.53	1.45	6.41	5.97	2.08	1.85
43495	875	0.79	0.77	4.11	4.01	1.49	1.48	6.26	6.22	1.99	1.98
43496	870	0.85	0.81	4.31	4.39	1.56	1.49	6.49	6.03	2.13	1.89
43499	870	0.81	0.77	4.27	4.21	1.49	1.45	6.21	6.03	1.96	1.86
43500	890	0.88	0.87	4.16	4.15	1.59	1.57	6.53	6.43	2.31	2.26

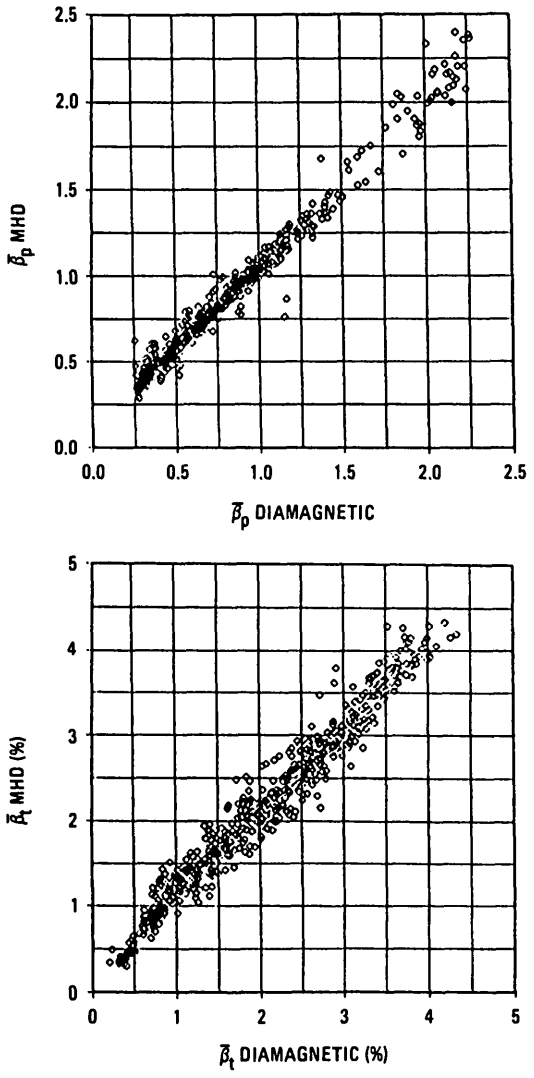

FIG.7. Comparison of diamagnetic beta values with MHD values.

Doublet III shots, reconstructed from the measured magnetic data using the EFIT code, are compared with those reconstructed using the GAQ code, which is based on the approach by Luxon and Brown [5] as described earlier. In the GAQ code, the current profile is parametrized non-linearly as given in Eq.(13). The two sets of values agree well with each other.

For Doublet III, in addition to the external poloidal magnetic field measurements, diamagnetic measurements are also available. From the diamagnetic measurements, $\bar{\beta}_p$ can also be determined by using the integral MHD equilibrium relationships [1–3] independent of those determined from the magnetic analysis based on poloidal magnetic field measurements alone. However, the latter type of magnetic analysis can only be used to determine $\bar{\beta}_p$ for elongated plasmas, whereas the diamagnetic measurements can be used to determine $\bar{\beta}_p$ for both circular and non-circular plasmas. For an isotropic plasma, the values of $\bar{\beta}_p$ from these two analyses should be identical. In Fig.7, the values of $\bar{\beta}_p$ and $\bar{\beta}_t$ determined from the EFIT code using this type of magnetic analysis are compared with the diamagnetically determined values for a vast number of recent Doublet III limited and diverted shots with $E > 1.15$, covering a wide range of plasma operating conditions. The two values of beta agree well with each other.

3.2. Sensitivity study

In this section, the effects of measurement errors on the reconstructed plasma shapes and global current profile parameters are studied. To simulate the measurement errors in actual experimental situations, the simulated signals at the measuring probes from the equilibrium calculations are randomly perturbed from −3% to 3%, an uncertainty level appropriate for Doublet III. The results of the reconstructed calculations are summarized in Table VI. Also shown are the exact values of the plasma parameters, the mean values of these parameters for this perturbed sample, and the root mean square (RMS) deviations of the parameters of this sample from the exact values. The RMS deviations of all geometry parameters are less than 3%, whereas $\bar{\beta}_t$, $\bar{\beta}_p$, ℓ_i and q_ℓ have RMS deviations of 6.0%, 6.3%, 3.2% and 4.8%, respectively.

3.3. Application to current profile evolution

In a first example, this method is used to detect the broadening and the contraction of the current profile due to the skin effect. In a particular Doublet III experiment studying current limits in the diverted Ohmic plasma, the total current I_0 was raised to 640 kA and held flat for about 100 ms (about one skin time) before being raised to 764 kA (Fig.8). During the flat-top phase the skin current built up on the initial ramp is expected to penetrate. The current profile should peak and the inductance ℓ_i should increase. During the second current ramp the current profile is expected to become broader owing to both the increased current and the skin effect, and ℓ_i should decrease. This behaviour was detected in the time history of ℓ_i given in Fig.8, reconstructed from the EFIT code using the method described above.

In the second example, the method is used to detect the broadening of the current profile during neutral-beam injection into a limited Doublet III

TABLE VI. COMPARISON OF PLASMA PARAMETERS RECONSTRUCTED FROM PERTURBED SIGNALS WITH THE EXACT VALUES

Case	a (cm)	E	$\bar{\beta}_t$	Ω (m^3)	q_ℓ	$\bar{\beta}_p$	ℓ_i	R_g (m)	Z_g (m)
Exact	40.46	1.59	3.60	6.93	2.51	0.81	0.78	1.45	0.74
1	40.39	1.57	3.62	6.86	2.44	0.80	0.78	1.45	0.75
2	40.09	1.61	3.97	6.90	2.51	0.90	0.73	1.45	0.74
3	40.40	1.55	3.41	6.74	2.38	0.76	0.79	1.45	0.76
4	40.43	1.56	3.48	6.80	2.39	0.76	0.79	1.45	0.76
5	40.85	1.61	3.19	7.09	2.65	0.73	0.82	1.44	0.74
6	40.59	1.53	3.49	6.73	2.36	0.77	0.80	1.45	0.77
7	40.61	1.61	3.52	7.04	2.63	0.82	0.78	1.45	0.74
8	40.65	1.56	3.44	6.85	2.43	0.77	0.80	1.45	0.76
9	40.55	1.61	3.46	7.01	2.57	0.79	0.78	1.45	0.74
10	40.39	1.56	3.52	6.77	2.34	0.76	0.78	1.45	0.75
Mean	40.49	1.58	3.51	6.88	2.47	0.79	0.78	1.45	0.75
RMS	0.21	0.03	0.22	0.14	0.12	0.05	0.02	0.00	0.01
RMS%	0.51	2.16	5.99	1.97	4.83	6.32	3.19	0.14	1.87

plasma. This effect is illustrated in the time history of ℓ_i, the plasma volume Ω, and the injected beam power given in Fig.9 for a limited dee-shaped Doublet III plasma. The plasma current I_0 was held roughly constant between 450 and 470 kA as the beam was injected into the plasma starting at about 620 ms. As the plasma is heated, ℓ_i drops from 0.84 to 0.74; simultaneously, $\bar{\beta}_t$ increases from 1.4% to 4.0%. This change in ℓ_i is about two times greater than the uncertainty in ℓ_i associated with the measurement errors. Figure 10 shows the toroidal current density in the horizontal plane passing through the

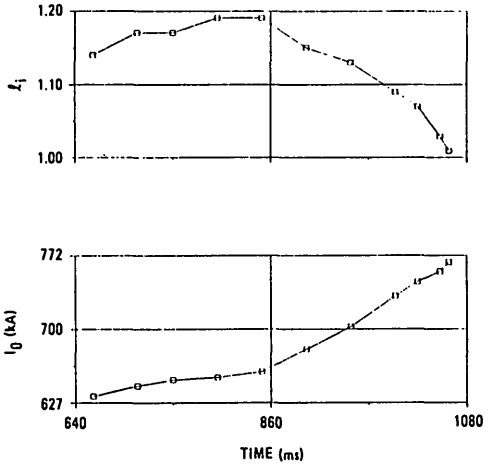

FIG.8. Evolution of ℓ_i and I_0 for a diverted Ohmic Doublet III plasma, shot 40959.

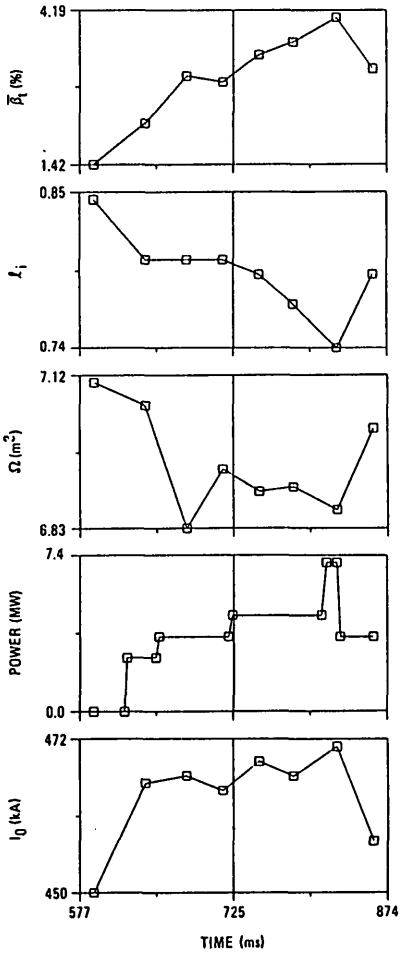

FIG.9. Time history of I_0, neutral-beam power, Ω, ℓ_i and $\bar{\beta}_t$, for a limited Doublet III plasma, shot 37937.

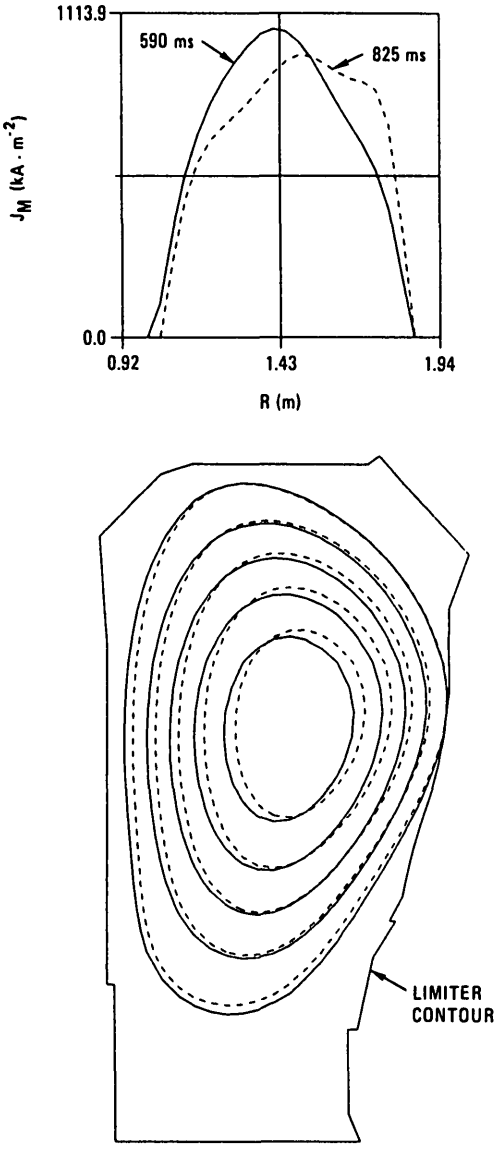

FIG.10. Reconstructed magnetic surfaces and J_M for a limited neutral-beam-injected Doublet III plasma, shot 37937, at 590 ms and 825 ms, shown by solid and dashed lines, respectively.

magnetic axis, J_M, and the magnetic surfaces at 590 ms and 825 ms. The solid lines are the reconstructed results at 590 ms and the dashed lines are the results at 825 ms. Since sawtooth activity was observed both before and during the beam injection, q_0 was constrained to a value of 0.95.

4. CONCLUSIONS

From the results of this study, it can be concluded that the plasma boundary shapes and global current profile parameters, such as $\bar{\beta}_p$, ℓ_i and q_ℓ, can be accurately and efficiently determined for non-circular plasmas from external magnetic measurements alone, as expected theoretically. For circular plasmas, an additional diamagnetic measurement is required. The values obtained depend only very weakly on the particular form of the current profile parametrization used and on the value of q_0 imposed. Secondly, the internal reconstructed magnetic surfaces depend more strongly on the value of q_0 imposed than on the particular form of the current parametrization used. From the external magnetic measurements and q_0, the internal magnetic surfaces can be relatively well determined, but not their derivatives. Finally, provided the current profile parametrization chosen models well the actual current distribution, from a knowledge of q_0 and the external magnetic measurements a current profile can be reconstructed which closely describes the gross features of the actual current distribution, but not its fine structure.

The amount of computational time required to perform a reconstruction using this method depends on the grid size used and on the relative error of ψ desired. A typical calculation on a VAX-11/780 computer, with a relative error of ψ less than 10^{-3}, requires 3–5 min of CPU time using the Green's function method on a 26 X 30 grid closely enclosing the plasma and 1–2 min using the Buneman's method on a 33 X 33 grid. Thus, this method is more appropriate for detailed after-shot analysis, which conveniently complements the between-shot analysis using the fast filament current method. For Doublet III, typically one to two time slices were easily analysed between every other shot using a VAX computer located in the control room and most of the data were analysed overnight.

Appendix

EVALUATION OF THE RESPONSE MATRIX $\vec{\vec{L}}$

Assuming a plasma current model of the form given in Eqs (4) and (5) and substituting into Eq.(9) yields

$$C_i^{(m+1)}(\bar{r}_i) = \sum_{n=1}^{n_e} G_{C_i}(\bar{r}_i, \bar{r}_{en}) I_{en}^{(m+1)} + \sum_{n=0}^{n_P} \alpha_n \times \int_{\Omega(m)} dR'dZ' 2\pi c R' G_{C_i}(\bar{r}_i, \bar{r}')(x^n - x^{n_P+1}) + \sum_{n=0}^{n_F} \beta_n \int_{\Omega(m)} dR'dZ' \frac{G_{C_i}(\bar{r}_i, \bar{r}')}{cR'}(x^n - x^{n_F+1}) \quad \text{(A.1)}$$

χ^2 can then be rewritten from Eq.(8) as

$$\chi^2 = \| \vec{\vec{L}}_1 \bar{y} - \vec{b}_1 \| + \| \vec{\vec{L}}_2 \bar{y} - \vec{b}_2 \| \qquad \text{(A.2)}$$

where $\vec{\vec{L}}_1$ denotes the response matrix relating the unknown coefficients to the measured field values, $\vec{\vec{L}}_2$ denotes the normalized constraint matrix, and $\vec{b}_1$ and $\vec{b}_2$ are the vectors containing the normalized measured field values and constraint values, respectively. Rearranging the terms in Eq.(A.2) then yields Eq.(12).

ACKNOWLEDGEMENT

This work was supported by the United States Department of Energy, under contract DE-AT03-84ER51044.

REFERENCES

[1] SHAFRANOV, V.D., Plasma Phys. **13** (1971) 757.
[2] BRUSATI, M., CHRISTIANSEN, J.P., CORDEY, J.G., JARRETT, K., LAZZARO, E., ROSS, R.T., Comput. Phys. Rep. **1** (1984) 345.
[3] LAO, L.L., St. JOHN, H., STAMBAUGH, R.D., PFEIFFER, W., Nucl. Fusion **25** (1985) 1421.
[4] SWAIN, D.W., NEILSON, G.H., Nucl. Fusion **22** (1982) 1015.
[5] LUXON, J.L., BROWN, B.B., Nucl. Fusion **22** (1982) 813.
[6] BLUM, J., LE FOLL, J., THOORIS, B., Comput. Phys. Commun. **24** (1981) 235;
BLUM, J., THOORIS, B., LE FOLL, J., presented at JET Workshop on Magnetic Measurements, 1980.
[7] McCLAIN, F.W., BROWN, B.B., GAQ: A Computer Program to Find and Analyze Axisymmetric MHD Plasma Equilibria, GA Technologies Rep. GA-A-14490 (1977).
[8] LACKNER, K., Comput. Phys. Commun. **12** (1976) 33.
[9] HELTON, F.J., WANG, T.S., Nucl. Fusion **18** (1978) 1523.
[10] JOHNSON, J.L., DALHED, H.E., GREENE, J.M., GRIMM, R.C., HSIEH, Y,Y., JARDIN, S.C., MANICKAM, J., OKABAYASHI, M., STORER, R.G., TODD, A.M.M., J. Comput. Phys. **32** (1979) 212.
[11] FORSYTHE, G.E., MALCOLM, M.A., MOLER, C.B., Computer Methods for Mathematical Computations, Prentice-Hall, Englewood Cliffs, NJ (1977).
[12] BERNARD, L.C., HELTON, F.J., MOORE, R.W., TODD, T.N., Nucl. Fusion **23** (1983) 1475.

(Manuscript received 23 April 1985
Final manuscript received 15 August 1985)